Malaria Detection and Classification in Microscopic Images

Group Number: G2B, Deep Learning Course Spring 2020

Ali Haider
Information Technology University
Arfa Software Technology Park, Ferozepur Road, Lahore
msee19006@itu.edu.pk

Ammar Rafique
Information Technology University
Arfa Software Technology Park, Lahore
phdee19002@itu.edu.pk
https://github.com/phdee19002/Malaria-Diagnosis-in-Microscopic-Images/

Abstract

Malaria is a common severe disease due to which millions suffer, primarily due to lack of timely diagnosis. More and more machine learning based expert systems are being developed and deployed, malaria diagnosis is one such candidate. Automated diagnosis can assist in remote areas, aside from time and cost savings. This works aims at improving parasite count accuracy, and parasite specie and disease stage diagnosis accuracy. Diagnosis has been performed to successfully detect and diagnose Plasmodium species as well as stage for Falciparum, Vivax, Malariae and Ovale. Three datasets were utilized which contained cell images as well as blood smear images. Three deep NN architectures were utilized. It was found that a single architecture does not yield best results on all three datasets. Unet base model produced best results for cell image classification at 89% accuracy while MASK RCNN produced best segmentation results for thin smear slide images with MAP 0.42.

1. Introduction

After more than 100 years of first diagnosis, malaria is still one of the deadliest diseases. It affects millions worldwide, every year. World Health Organization states on its website that in 2018 alone, 228 million were infected and 0.4 million died [1]**Error! Reference source not found.**. For comparison, 5.5 million confirmed cases of infection with 0.3 million deaths have occurred due to COVID-19 [2], up till May 2020, which needs no introduction. Although curable, the fact that majority of deaths due to malaria are children (67% deaths under the age of 5) does not make it less deadly. In countries such as Pakistan, despite availability of cure diagnosis is the bottleneck. According to the directorate of malaria control Pakistan, millions are at the risk of malaria[3]. The malaria is especially prevalent in the far reach areas of Baluchistan, Sindh and western border [3].

Analysis of stained blood samples under bright field microscopy is considered is as gold standard for malaria identification [4]. The procedure includes counting and classification of parasite type and stages by trained technician. The process is time consuming and requires highly trained professionals. Hence, in this project we aim at automating the process of malaria analysis using microscopic images of thin blood smears.

1.1. Motivation

This project aims at automating the process of malaria analysis using microscopic images of thin blood smears. It will lower the analysis cost and time by many folds. By this project we will be able to help the technician or end the need of the technician on every single case for the malaria diagnosis.

1.2. Proposed Solution

In this project we aim at estimating the degree of parasitemia (degree of parasitic infection), detect and classify the parasite specie with their stages. There are four different species of malaria parasite Falciparum (75% occurrence), Vivax (20% occurrence)[5], Malariae and Ovale. Each type has different stages called Ring, Trophozoite, Schizont and Gametocyte[6].

In order to estimate the degree of parasitemia and infected cell segmentation we will be using fully convolutional networks[7][8], and in order to classify the stage and type of parasite specie we will evaluate different convolutional neural network architectures.

For the stated purpose we will be utilizing datasets from[9][10][11].

1.3. Objective

The objective of the project is to design a solution capable of utilizing microscopic images of blood samples, for the purpose of:

- Identifying the degree of parasitemia in stained blood sample.
- Classify the different parasite species.
- Classify the parasite stage.
- Comparative analysis of different networks on different datasets.

.

2. Literature Review

This section discusses the role of microscopic images in malaria diagnosis and previous works, that attempted to perform automated malaria diagnosis.

2.1. Malaria

Malaria is disease caused by Plasmodium parasite. It is transmitted through bite of Female Anopheles mosquito. The Mosquito bite releases Plasmodium parasite sporozoite form, which is inactive for human cells and remains undetected. Once transmitted, the parasite enters the blood stream and travels to the liver. In the liver the sporozoites mature, in 10 to 15 days depending upon Plasmodium specie, to form merozoite which can infect human cells. Then the infected liver cells burst to release new copies which then invade the RBCs (red blood cells). In 2-3 day cycle, the blood cell bursts again and parasites are released to infect more cells. At this stage of the disease, malaria symptoms appear. The cycle keeps repeating until recovery or death. This is the reason why microscopic images of blood samples can be utilized in identifying the type of Plasmodium and the stage of infection.

When a blood sample is to be analyzed, it is stained by a suitable reagent, such as Giemsa stain, which marks the Plasmodium. The stained blood is put on a slide and viewed using a microscope. The gold standard is to have an expert medical professional diagnose using microscopic images, the specie of parasite and the stage of infestation. Figure 1 and Figure 2 show blood cell appearance for two of the Plasmodium specie and infection stage. The variation in staining for same specie stages and similarity among different specie stages can be seen, which can be a source of confusion even for human experts. Moreover, these are not discrete stages and transition stages can be further confusing to classify. Figure 3 is shown as an example case.

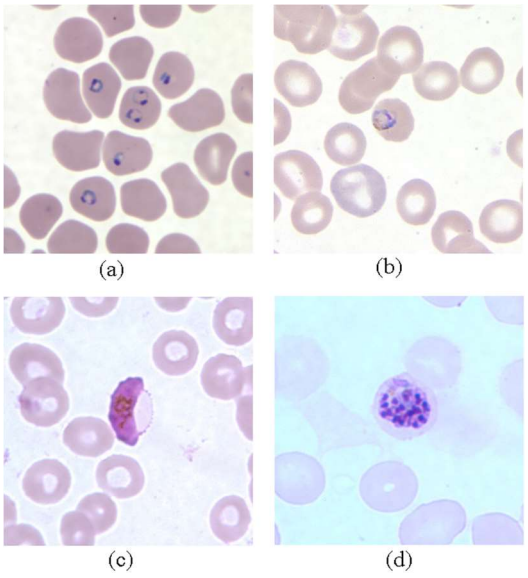

Figure 1: Plasmodium Falciparum 4 stages of infection. (a) Ring, (b) Trophozoite, (c) Gametocyte, (d) Schizont[12].

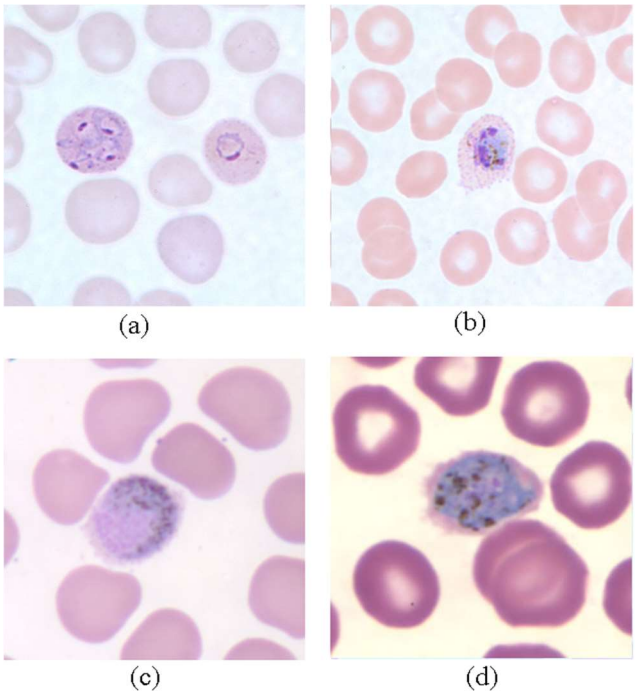

Figure 2: Plasmodium Ovale 4 stages of infection. (a) Ring, (b) Trophozoite, (c) Gametocyte, (d) Schizont[12].

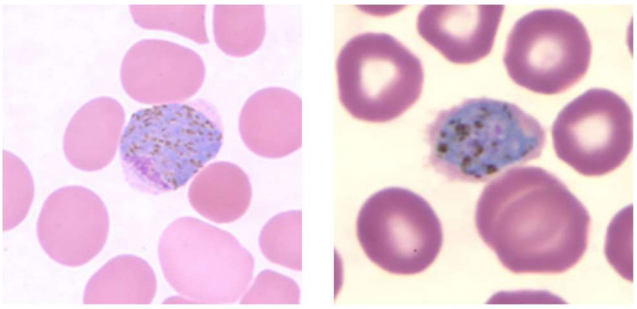

(a) (b)

Figure 3: (a) Vivax Gametocyte, (b) Ovale Schizont[12].

The previous works on automated diagnosis techniques utilize image processing techniques, combination of image processing and machine learning techniques or deep learning techniques, applied onto microscopic images.

2.2. Image Processing Techniques

Brief review of image processing techniques and combination with machine learning techniques is compiled in Table 1 :

Technique	Classification or Detection	Achieved Result
Using infected cell data and MLP. RBC size, parasite count and shape etc. [13]	P. Falciparum, Vivax and Malariae Classification	89.8%
Logistic regression-based thresholding [14]	Detection	88.7%
Using Bayesian Classifier for thresholding [15]	Detection	93.3%
Wavelet feature extraction and PCA with 3 layer Neural Network [16]	P. Falciparum and Vivax Classification	77.1%
Image processing for feature extraction and Adaptive Resonance Theory Network [17]	Detection	94.4%
ANN for morphological operation parameter optimization [18]	P. Falciparum and Vivax Classification.	73.5%

Table 1: Image Processing techniques applied for malaria diagnosis.

Image processing techniques are usually clever hand-crafted methods that can tackle a somewhat robust but narrow situation and not well generalized. Following situations are naturally inherent to the problem of microscopic pathogen diagnosis, which result in reduced performance:

- Visual variation due to staining types
- Visual variation due to microscope lighting conditions
- Variation in morphology due to genetic diversity
- Variation in morphology due to mutations
- Limited understanding of the target by the humans involved.

Hence, the deep learning techniques which involve end to end training with minimal prejudiced preprocessing.

2.3. Related Work and Deep Learning Techniques

Recent deep learning techniques utilized in diagnosis of malaria are listed in Table 2. Some techniques not applied to malaria diagnosis yet but otherwise successful in other image based medical diagnosis have also been included.

Reference	Technique	Detection / Classification	Dataset Link	Achieved Result
[19]	Cell images fed to transfer learning AlexNet+ SVM	Detection	[11]	91.99 %
	Cell images fed to new 17-layer CNN end-to-end			97.37 %
[20]	Blood smear field of view images FRCNN transfer learning from ImageNet	Classification P. Vivax stages	[10]	59%
	Blood smear field of view images, 2-stage FRCNN and AlexNet, transfer learning from ImageNet	Classification P. Vivax stages		98%
[21]	Cell images fed to transfer learning AlexNet+ SVM	Detection	[22]	91.66 %
	Cell images			96.18

	fed to LeNet-5			%
	Cell images fed to AlexNet			95.79 %
	Cell images fed to GoogLeNet			98.13 %
[23]	Brain MRI to Unet modified with added bypass links	Brain Tumor Segmentation	Not malaria	0.81*
[8]	Brain and Liver MRI to Unet based on DenseNet-161	Brain and Liver Tumor Segmentation		0.937 * and 0.982 *
*	DSC = Dice Similarity Coefficient for volumetric medical image			

Table 2: Recent Deep Learning techniques applied for malaria diagnosis.

Techniques in [19]**Error! Reference source not found.** and [23] were applied on the same datasets as this project. Therefore, these works have been considered guidelines and benchmarks for our work. Further discussion is in section **4.**

IT should be noted that reported results are much more promising than obtained using image processing techniques. However, deep learning techniques suffer from drawbacks of their own. Such as:

- High computational cost i.e. processing power and time
- Large dataset required for training

Case of malaria diagnosis suffers particularly from the second problem. Datasets are not large or do not cover full range of case possibilities. High computational cost is less of a problem due to availability of remote access HPC clusters such as Google Colab, which was utilized in this work.

3. Dataset Description

Four datasets were utilized in this project. Each dataset is discussed in the following.

Dataset A: Thin blood smear slides from 150 infected persons and 50 uninfected persons were prepared by Chittagong Medical College Hospital, Bangladesh. The slides were stained using Giemsa reagent and images were taken using smart phone camera attached to microscope. The images were then cropped into images of individual cells. The images were then annotated by expert slide reader at Mahidol-Oxford Tropical Medicine Research Unit in Bangkok, Thailand. A dataset of 27560 images was finally formed, 13780 infected cells and 13780 uninfected cells[11]. The plasmodium specie identified was only Falciparum and no information on stage of infection was provided in the image labels. Figure 4 below shows two samples from the dataset.

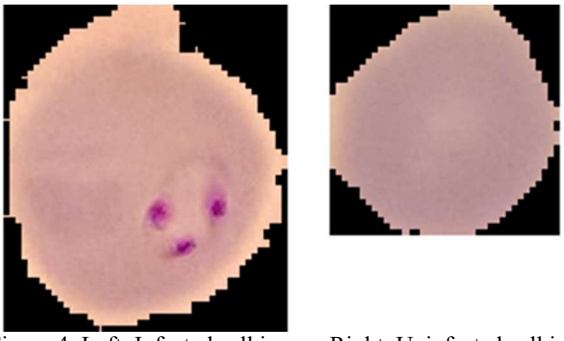

Figure 4: Left: Infected cell image. Right: Uninfected cell image.

Please note that each image is roughly 130 by 150pixel in resolution.

Dataset B: This dataset is provided by Broad Institute of MIT. It is made publicly available at the Broad Bioimage Benchmark Collection website[10]. The images are of Giemsa stained thin blood smears of Plasmodium Vivax specie infection only. Dataset was labelled by Stefanie Lopes, a malaria researcher at the Dr. Heitor Vieira Dourado Tropical Medicine Foundation hospital. Bounding box annotations are provided in a "json" file. The bounding box annotations identify infected RBCs, Leukocytes and the stage of infection too in the infected cells. Uninfected cells are not annotated which are claimed to be almost 95% of the total cell instances. Also, the ambiguous samples are separately marked as "difficult". A sample is shown in Figure 5. In total, there are 1380 images.

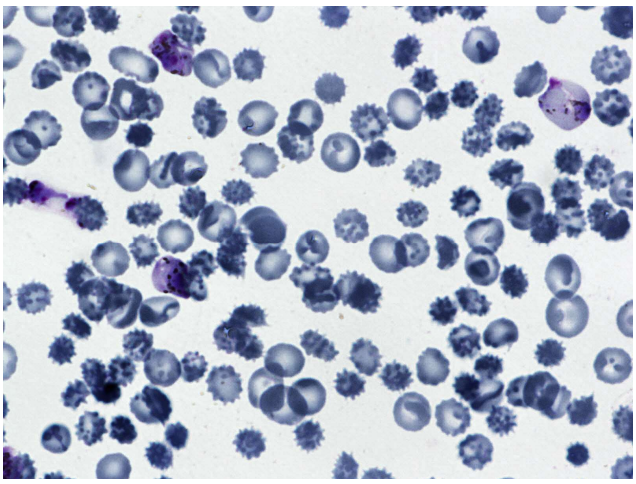

Figure 5: Dataset B sample image.

Dataset C: This dataset is available at [9] and was published along with [6] which describes the dataset. The name of image as well as ground truth contains the stage label while each plasmodium specie is grouped in a separate folder. The ground truths are "black and white" images, infected cell area has white mask, rest is black. If more than one stage is identified then image has more than one stage label. Samples are shown in Figure 6 and Figure 7. Total number of samples are 210, of which 104 belong to Plasmodium Falciparum specie, 40 Vivax, 29 Ovale and 37 Malariae.

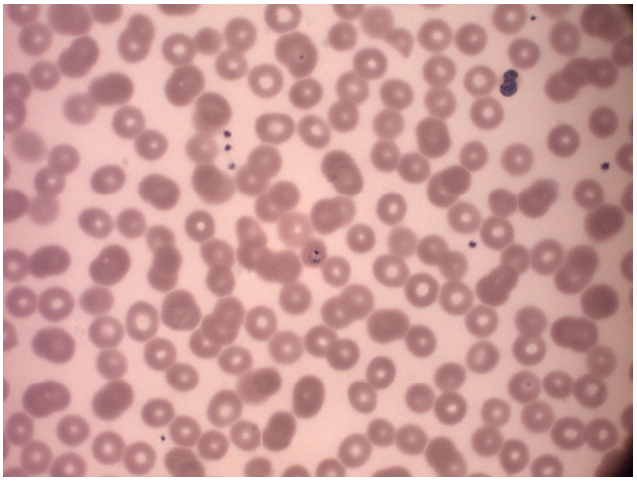

Figure 6: Dataset C sample image.

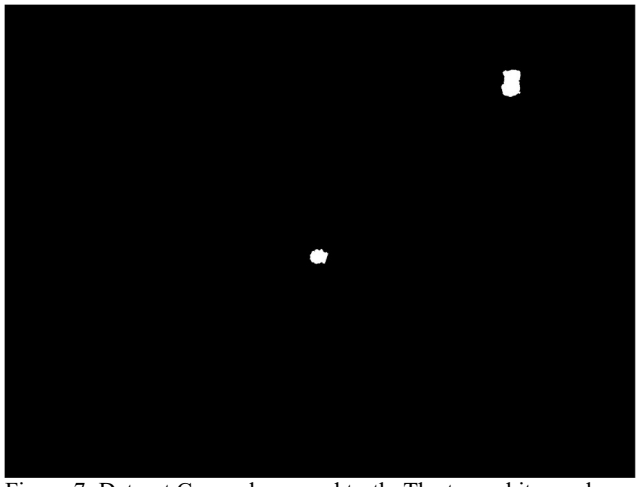

Figure 7: Dataset C sample ground truth. The two white masks are infected cells.

All these datasets have either only one specie or class imbalance. Even if all the datasets are merged, the class imbalance will not decrease but rather increase. However, these are publicly available and hence follow up work and verifying results is possible.

4. Deep CNN

For this project we utilized multiple types of architectures and compared them for the best results. We used three architectures which are Unet based model, Yolov3 based implementation and Mask RCNN based detector.
UNET based Implementation

4.1. UNET based implementation

The Unet based implementation includes multiple networks cascades to localize the cells and classify them.

4.1.1 Network Architecture

The network includes Unet to generate the segmentation mask, followed by the contour detection to create the bounding box and last is the traditional CNN classifier to classify the bounding box regions extracted earlier. Figure 8: Architecture for Unet based implementation is shown.,

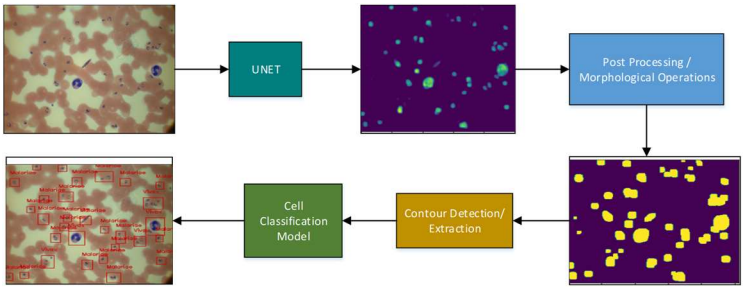

Figure 8: Architecture for Unet based implementation

The Unet used here is a modified version of the standard Unet architecture, shown in the appendix A Figure 1A. It includes four max pooling layers for downscaling and four transpose convolution layers for upscaling. The output of the UNET is subjected to different morphological operations to remove the noise. The image is then thresholded to obtain a binary mask. The contour detection algorithm is used to create the bounding box for the regions of interest in binary mask images. The ROI of interest are then extracted and classified using traditional classifier networks.

4.1.2 Training

For the first step the network architecture is trained for dataset C. Training aims at classifying the infected cells into plasmodium classes. Initially the UNET is using infected images and corresponding ground truth mask images. The UNET is trained using Stochastic gradient descent with learning rate of 0.001 and momentum of 0.9. A weight decay factor was used with the value of 10^{-5}. The loss function used to train the UNET architecture is mean square error (MSE). In Figure 9 UNET loss curve shown. For classification we used VGG16 model with the cross entropy loss function. The training accuracy and loss curves for the classifier are in the Figure 10 and Figure 11.

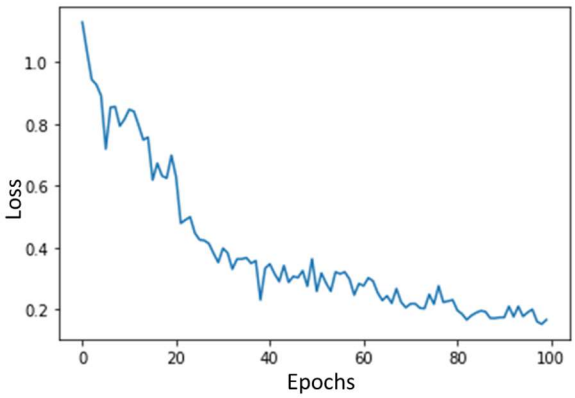

Figure 9 UNET loss curve

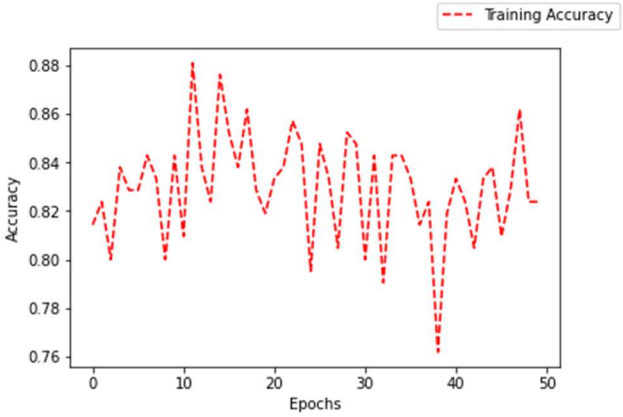

Figure 10 Vgg16 training accuracy curve

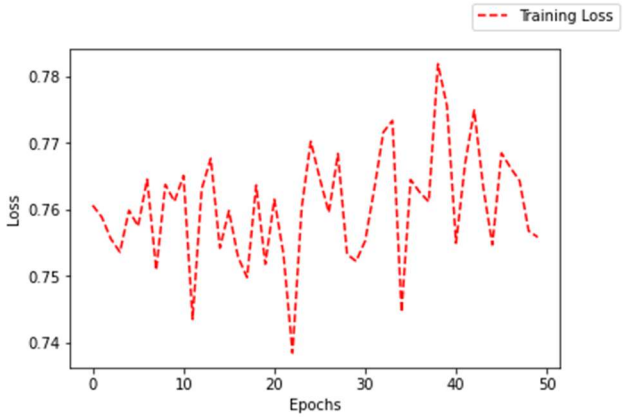

Figure 11 Vgg16 training loss curve

The classifier achieved a test accuracy of 67%.

The same architecture was trained on the Dataset C to classify the stage of the plasmodium vivax. The dataset was trained in the same way as we did in the dataset A. The ground truth mask against the infected images were generated using square annotations. The loss curve for the model is in the Figure 12.

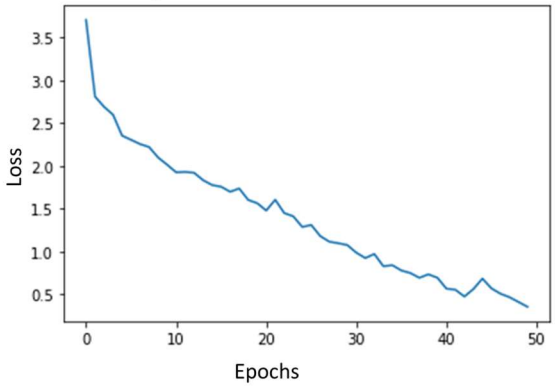

Figure 12 Loss curve for UNET trained on dataset B

The classifier used for the dataset B is modified resnet18 providing the promising results. The dataset is trained using focal loss for complete model. The model is trained for 10 epochs, learning rate 0.001, Adam optimizer. The value of alpha = 0.2 and gamma = 2 for focal loss. The training accuracy and validation curves are in Figure 13.

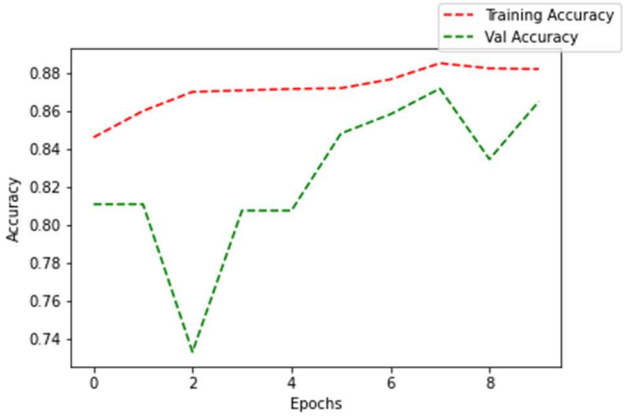

Figure 13 Accuracy curves for Modified Resnet18

The loss curves for the accuracy and validation are in the Figure 14

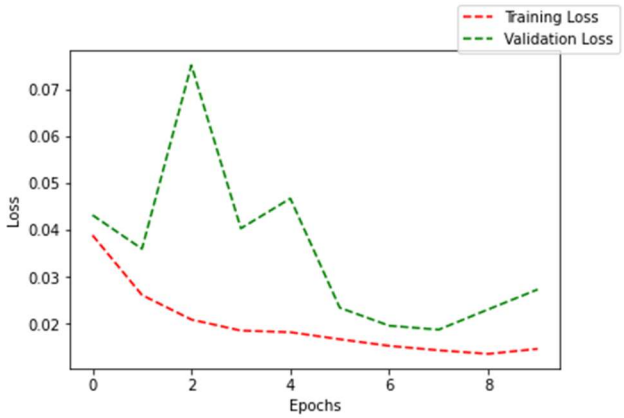

Figure 14 Loss curves for Modified Resnet18

4.1.3 Results

Results for dataset C are as follows.

The IOU achieved for the detected results is 0.8232 and mean square pixel loss is 0.1302.

The accuracy achieved by the vgg16 is 67% for the test set.

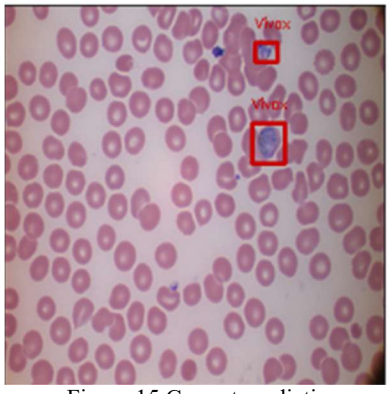

Figure 15 Correct prediction

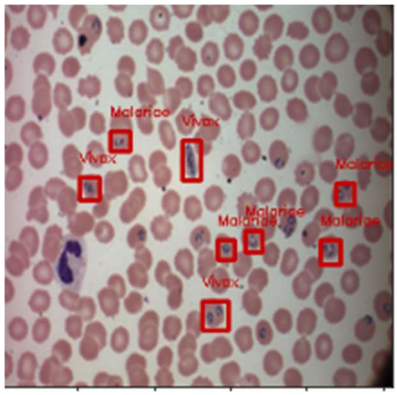

Figure 16 Partial prediction

The detection made by UNET and contour detection is 89% but the real issue lies in the classifier resulting in the overall bad classifications.

The UNET based implementation for dataset B have very bad results due to square annotations based results.

4.2. YoloV3 based implementation

Yolov3[24] is one of the famous object detector models. It is a modification of yolo[25] which uses a single unified neural network making it extremely fast. In our case we trained yolo for binary cross entropy loss and focal loss. We observed a clear improvement due to the focal loss.

4.2.1 Network Architecture

Yolov3 is consist of backbone network called darknet53, up sampling layers and detection layers called yolo layers. The darknet53 consist of 53 convolution layers. The yolov3 detects the objects at different 3 scales allowing it to detect smaller objects. We used the standard yolov3 architecture.

4.2.2 Training

We trained yolov3 for binary cross entropy lose and focal loss for dataset B. The overall results when using the focal loss are much better as compared to the binary cross entropy loss.

Binary cross entropy is unable to deal with the class imbalance present in our dataset. Our dataset consists of 5 classes. Which are difficult, gametocyte, ring, schizont, trophozoite. The difficult class cells have not proper affiliation with any class. The model is trained using a batch size of 64. The optimizer used is SGD with learning rate of 0.01 and momentum of 0.9. The loss curve for yolov3 is in Figure 17,

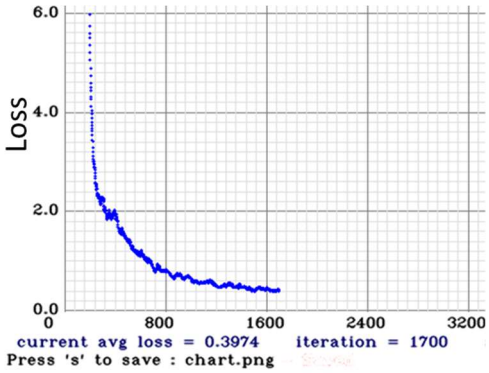

Figure 17 Yolov3 BCE loss curve

The focal loss provides the better result for the imbalanced data. The alpha = 0.5 and gamma = 2. The other parameters were same as before, the loss curve for the focal loss based implementation is in Figure 18,

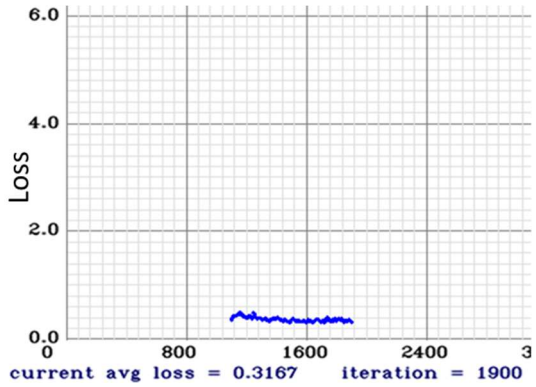

Figure 18 Focal loss curve for yolov3

The loss reduced due to the using focal loss.

4.2.3 Results

The yolov3 when trained with binary cross entropy loss obtained lesser accuracy as compared to the focal loss. The model obtained a total of 0.1756 or 17.56 % mean average person IOU of 0.5. The results for the prediction are in Figure 18. The yolo have missed some of the infected cells and more over it have misclassified the cells stage to trophozoite but actually they are at ring stage. As shown in the Figure 19,

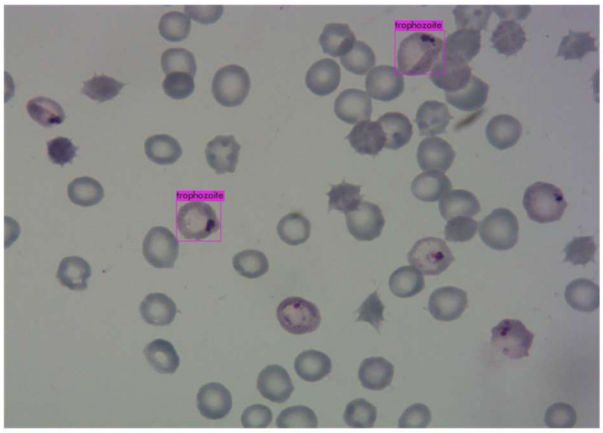

Figure 19 Yolov3 with BCE results

When yolov3 is trained on the focal loss the mean average precision achieved for the test dataset is 28.23% which is about 11% more than the one obtained in BCE version. The results for focal loss[26] are shown in Figure 20. The focal loss misses/misclassify some infected cells but classified some cells correct and it could be directly linked to the better mean average precision in comparison to the BCE loss.

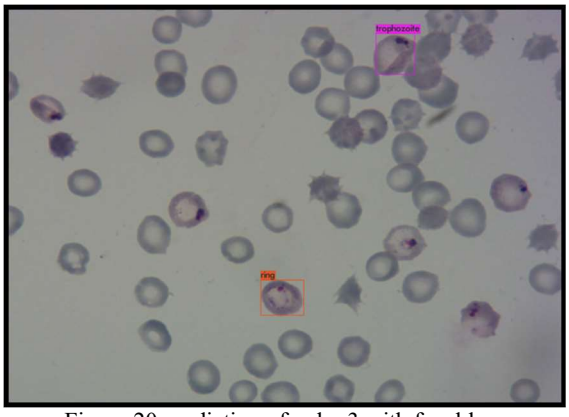

Figure 20 prediction of yolov3 with focal loss

4.3. Mask RCNN

Mask R-CNN[27] is an architecture for object detection and classification. It generates the mask, bounding box and classes against an input. It preserves semantic information regarding the object as a result, it outperforms many single stage detectors. It is like faster RCNN [28] with an addition of fully convolutional network (FCN) predicting the masks.

4.3.1 Architecture

There are two stages in Mask RCNN[27]. First stage generates the proposal about the existence of object and second stage classify, predict mask and refines the bounding boxes. The simplified architecture of Mask RCNN is shown in the Figure 21,

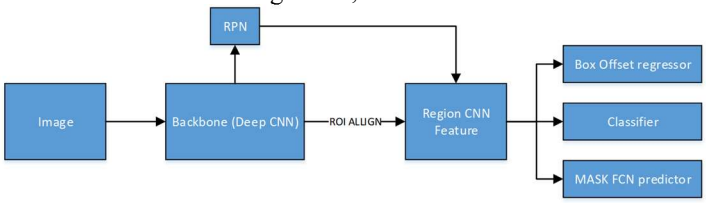

Figure 21 Architecture of Mask RCNN

We used resnet101 as backbone network for the Mask RCNN.

4.3.2 Training

The network is trained on the dataset BBBC041 using Resnet101 as backbone. The network was trained using SGD for learning rate of 0.001 and momentum of 0.9 with 1000 iterations per epochs. Training achieved an average mean precision of 0.67 or 67% on training dataset.

4.3.3 Results

The Mask R CNN obtained a mean average precision of 0.4217 or 42.17 %. The performance of the model can be further enhanced with increased model training and using the specialized loss function. For now, we have trained model with the traditional loss function. Some of the

detection results are shown in the Figure 22 and corresponding ground truths in Figure 23,

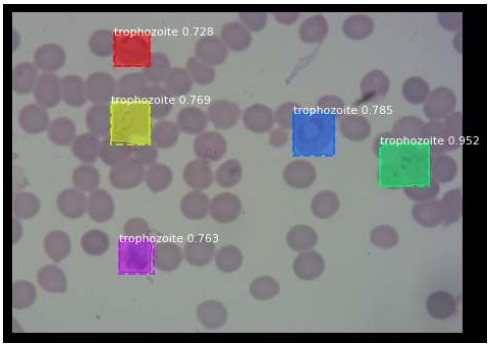

Figure 22 Mask RCNN results

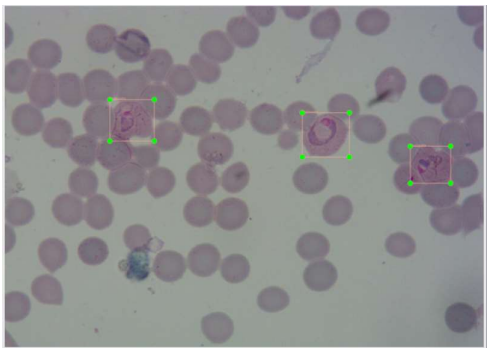
Figure 23 MASK RCNN ground truth

The model has some false detection issue and is more partial towards the trophozoite due to the class imbalance issue.

Table 3

	Methods	Dataset	Loss	IOU	MAP
1	Yolov3	Dataset B	BCE	0.5	0.1756
2	Yolov3	Dataset B	Focal loss	0.5	0.27
3	Mask RCNN	Dataset B	CE loss	0.5	0.4217

5. Conclusion

UNET based implementation is more fine for the plasmodium classification due to very limited dataset availability. The Unet based implementation have detection accuracy of 89% with better IOU equal to 0.8, The classification performance is limited by the classifiers accuracy. The model faces issue while dealing with different staining types. The accuracy is limited up to a point due to separate models. It works fine for dataset C. The Unet based do not provide better results because of rectangular annotations in the case of dataset B.

As show in the Table 3, The yolov3 have provided a better result with focal loss but is unable to give deal with the larger/ closer objects.

The stage classification is best done by the Mask RCNN. It provided the best mean average precision of all the networks evaluated here. Hence, one architecture was not perfected for all datasets.

This work does did not achieve state of the art results but it provides insight into datasets and deep CNN architectures, very different from each other. More work is needed to achieve an architecture suited to all datasets, especially in developing a larger dataset which covers all species and stages with sufficient examples for each label.

References

[1] "Malaria." https://www.who.int/news-room/fact-sheets/detail/malaria (accessed Jul. 09, 2020).

[2] "Coronavirus disease (COVID-19)." https://www.who.int/emergencies/diseases/novel-coronavirus-2019 (accessed Jul. 09, 2020).

[3] "MALARIA CONTROL PROGRAM IN PAKISTAN." http://dmc.gov.pk/index.php?option=com_content&view=article&id=55&Itemid=88-title=MALARIA (accessed May 28, 2020).

[4] C. W. Pirnstill and G. L. Coté, "Malaria Diagnosis Using a Mobile Phone Polarized Microscope," *Sci. Rep.*, vol. 5, no. 1, pp. 1–13, Aug. 2015, doi: 10.1038/srep13368.

[5] B. Nadjm and R. H. Behrens, "Malaria: An Update for Physicians," *Infectious Disease Clinics of North America*, vol. 26, no. 2. Infect Dis Clin North Am, pp. 243–259, Jun. 2012, doi: 10.1016/j.idc.2012.03.010.

[6] A. Loddo, C. Di Ruberto, M. Kocher, and G. Prod'hom, "Mp-idb: The malaria parasite image database for image processing and analysis," in *Lecture Notes in Computer Science (including subseries Lecture Notes in Artificial Intelligence and Lecture Notes in Bioinformatics)*, Sep. 2019, vol. 11379, pp. 57–65, doi: 10.1007/978-3-030-13835-6_7.

[7] W. Xie, J. A. Noble, and A. Zisserman, "Microscopy cell counting and detection with fully convolutional regression networks," *Comput. Methods Biomech. Biomed. Eng. Imaging Vis.*, vol. 6, no. 3, pp. 283–292, May 2018, doi: 10.1080/21681163.2016.1149104.

[8] X. Li, H. Chen, X. Qi, Q. Dou, C. W. Fu, and P. A. Heng, "H-DenseUNet: Hybrid Densely Connected UNet for Liver and Tumor Segmentation from CT Volumes," *IEEE Trans. Med. Imaging*, vol. 37, no. 12, pp. 2663–2674, Dec. 2018, doi: 10.1109/TMI.2018.2845918.

[9] "GitHub - andrealoddo/MP-IDB-The-Malaria-Parasite-Image-Database-for-Image-Processing-and-Analysis: MP-IDB is the public image dataset described in the following article: https://link.springer.com/chapter/10.1007/978-3-030-13835-6_7." https://github.com/andrealoddo/MP-IDB-The-Malaria-Parasite-Image-Database-for-Image-

Processing-and-Analysis (accessed Jul. 09, 2020).
[10] "BBBC041: P. vivax (malaria) infected human blood smears." https://data.broadinstitute.org/bbbc/BBBC041/ (accessed Jul. 09, 2020).
[11] "Malaria Datasets | National Library of Medicine." https://lhncbc.nlm.nih.gov/publication/pub9932 (accessed Jul. 09, 2020).
[12] "CDC - DPDx - Malaria." https://www.cdc.gov/dpdx/malaria/index.html (accessed Jul. 09, 2020).
[13] "Classification Of Malaria Parasite Species Based On Thin Blood Smears Using Multilayer Perceptron Network - Dialnet." https://dialnet.unirioja.es/servlet/articulo?codigo=5823185 (accessed Jul. 09, 2020).
[14] S. Mandal, A. Kumar, J. Chatterjee, M. Manjunatha, and A. K. Ray, "Segmentation of blood smear images using normalized cuts for detection of malarial parasites," in *Proceedings of the 2010 Annual IEEE India Conference: Green Energy, Computing and Communication, INDICON 2010*, 2010, doi: 10.1109/INDCON.2010.5712739.
[15] D. Anggraini, A. S. Nugroho, C. Pratama, I. E. Rozi, Aulia Arif Iskandar, and Reggio Nurtanio Hartono, "Automated status identification of microscopic images obtained from malaria thin blood smears," in *Proceedings of the 2011 International Conference on Electrical Engineering and Informatics, ICEEI 2011*, 2011, doi: 10.1109/ICEEI.2011.6021762.
[16] L. Yunda, A. Alarcón, and J. Millán, "Automated Image Analysis Method for p-vivax Malaria Parasite Detection in Thick Film Blood Images," *Sist. y Telemática*, vol. 10, no. 20, p. 9, Mar. 2012, doi: 10.18046/syt.v10i20.1151.
[17] M. L. Chayadevi and G. T. Raju, "Usage of ART for Automatic Malaria Parasite Identification Based on Fractal Features," 2014.
[18] S. T. Khot and R. K. Prasad, "Optimal computer based analysis for detecting malarial parasites," in *Advances in Intelligent Systems and Computing*, 2014, vol. 327, pp. 69–80, doi: 10.1007/978-3-319-11933-5_9.
[19] Z. Liang *et al.*, "CNN-based image analysis for malaria diagnosis," in *Proceedings - 2016 IEEE International Conference on Bioinformatics and Biomedicine, BIBM 2016*, Jan. 2017, pp. 493–496, doi: 10.1109/BIBM.2016.7822567.
[20] J. Hung *et al.*, "Applying Faster R-CNN for Object Detection on Malaria Images," Apr. 2018, Accessed: Oct. 15, 2019. [Online]. Available: http://arxiv.org/abs/1804.09548.
[21] Y. Dong *et al.*, "Evaluations of deep convolutional neural networks for automatic identification of malaria infected cells," in *2017 IEEE EMBS International Conference on Biomedical and Health Informatics, BHI 2017*, Apr. 2017, pp. 101–104, doi: 10.1109/BHI.2017.7897215.
[22] "PEIR-VM: IPLab11Malaria." https://peir-vm.path.uab.edu/debug.php? slide=IPLab11Malaria (accessed Jul. 09, 2020).
[23] H. Dong, G. Yang, F. Liu, Y. Mo, and Y. Guo, "Automatic Brain Tumor Detection and Segmentation Using U-Net Based Fully Convolutional Networks," p. 1, May 2017, Accessed: Jul. 09, 2020. [Online]. Available: http://arxiv.org/abs/1705.03820.
[24] J. Redmon and A. Farhadi, "YOLOv3: An Incremental Improvement," Apr. 2018, Accessed: Jul. 09, 2020. [Online]. Available: http://arxiv.org/abs/1804.02767.
[25] J. Redmon, S. Divvala, R. Girshick, and A. Farhadi, "You only look once: Unified, real-time object detection," in *Proceedings of the IEEE Computer Society Conference on Computer Vision and Pattern Recognition*, Dec. 2016, vol. 2016-December, pp. 779–788, doi: 10.1109/CVPR.2016.91.
[26] T.-Y. Lin, P. Goyal, R. Girshick, K. He, and P. Dollár, "Focal Loss for Dense Object Detection," *IEEE Trans. Pattern Anal. Mach. Intell.*, vol. 42, no. 2, pp. 318–327, Aug. 2017, Accessed: Jul. 09, 2020. [Online]. Available: http://arxiv.org/abs/1708.02002.
[27] K. He, G. Gkioxari, P. Dollar, and R. Girshick, "Mask R-CNN," in *Proceedings of the IEEE International Conference on Computer Vision*, Dec. 2017, vol. 2017-October, pp. 2980–2988, doi: 10.1109/ICCV.2017.322.
[28] S. Ren, K. He, R. Girshick, and J. Sun, "Faster R-CNN: Towards Real-Time Object Detection with Region Proposal Networks," Jun. 2015, Accessed: Jul. 09, 2020. [Online]. Available: https://arxiv.org/abs/1506.01497v3.